THERMAL DIFFUSION AND FLOW PROPERTY OF CO_2/CH_4 IN ORGANIC NANOPORES WITH FRACTAL ROUGH SURFACE

by

Jian HE[a], Yang JU[a,*], and Peng HOU[b]

[a] State Key Laboratory for GeoMechanics and Deep Underground Engineering, China University of Mining and Technology, Xuzhou, China
[b] Department of Industrial and Physical Pharmacy, Purdue University, West Lafayette, Ind., USA

Original scientific paper
https://doi.org/10.2298/TSCI180912226H

The kerogen is rich in complex pore networks with a random rough surface, which is a factor controlling the thermal diffusion and flow property of gases. In this work, we construct organic-rich nanopore with fractal surfaces by inserting and deleting carbon atoms. The adsorption ability, thermal diffusion property, and flow velocity of CO_2/CH_4 in the nanopore are analyzed using with molecular simulations. The results showed that the adsorption capacity of CO_2 is nearly twice that of CH_4, which is decided by adsorption enthalpy, whereas the maximum thermal diffusion ability of CO_2 is only 23.7% that of CH_4. With external pressure gradients imposed on the system, the flow speed of CO_2 was lower than that of CH_4 for nanopores with different roughness. These findings provide a theoretical basis for the feasibility of CO_2 exploitation of shale gas.

Key words: *nanopores, diffusion, flow, thermodynamic*

Introduction

In the past few decades, significant amount of business and research investments have been directed towards the extraction and investigation of shale resources [1]. However, with the extensive application of this technology, there is wide concern regarding the effects of this technology on the environment, water resources, and human life [2]. Thus, the exploration of non-hydraulic fractures, such as supercritical CO_2 or liquid N_2 fracture systems, has been receiving considerable attention [3].

The non-aqueous technologies are still in the research stage, restricted to the complex thermodynamic state and the geographical conditions of the shale reservoirs. The molecular simulations have been used to study of the adsorption and transportation of the gases in nanopores [4]. Moreover, the permeability of the gases has been studied using molecular dynamics (MD) simulations considering the nanopores in the shale as simplified nanotubes or slit nanopores with a smooth surface [5]. However, kerogen, which is the main sources of the shale gas, exhibits a complex pore networks and extremely high roughness values from the macro-scale to molecular-scale [6].

The roughness using the simplified and regular patterns to describe the actual surface structure at the nanoscale was considered in [7]. The roughness is an important factor affecting the fluid flux through micro/nanopores [8]. However, as an amorphous structure, the surface of

* Corresponding author, e-mail: juy@cumtb.edu.cn

the nanopores in the kerogen lacks of the high-level symmetry or novel geometric patterns. It is increasingly important for understanding the flow of gases in the pore networks of kerogen to construct a random rough surface at the molecular scale.

The fractal function has a self-affine property and shows similarity for multi-scale structures. It can be used to describe the natural surface and capture the different scales of property [9]. In this article, to understand the thermal diffusion property and flow speed of CO_2/CH_4 in real kerogen pores, a fractal surface controlled by Weierstrass-Mandelbrot (W-M) function [10] will be considered to describe the topography of kerogen, and the isolated carbon atoms will be used to represent the skeleton of the kerogen. The carbon atoms are inserted into a box controlled by the W-M function. Moreover, the adsorption ability of CO_2/CH_4 is determined from a GCMC simulation, and the dynamic information of CO_2/CH_4 contained in these models is extracted from an MD simulation.

Models and methods

Simulation set-up for the rough nanopores

The separated single carbon atoms were used to represent the walls of a kerogen nanopore system in shale. Three different types of the rough surfaces were created based on the W-M equation [10], which is given:

$$z(x) = G^{(D-1)} \sum_{n=n_1}^{\infty} \frac{\cos\left(2\pi\gamma^n x\right)}{\gamma^{(2-D)n}} \tag{1}$$

where $G = 0.2$ nm is the roughness amplitude, D – the fractal dimension of the roughness profile (here, we take $D = 1.1$, $D = 1.3$, and $D = 1.5$) and $\gamma = 1.3$ – the factor, which is controlling the frequency density. For a real roughness profile, a fractal characterization of the rough surface based on eq. (1) can be computated once the fractal dimension has been determined. The typical simulation cell set-up is shown in fig. 1.

A face centre cubic lattice structure with a lattice constant of 3.34 Å is used in this model. The roughness of the nanopore surface is characterized by fractal dimensions of 1.1, fig. 1(a), 1.5, fig. 1(b), and 1.3, fig. 1(c). An increase in the fractal dimension leads to a variation of the roughness. The box sizes in the x (parallel to the flow direction) and y/z (perpendicular to the flow direction) directions are given as 6.8 nm and 5.1-1.7 nm, respectively. A periodic boundary is applied in all the directions to solve the scale problem in the MD simulation.

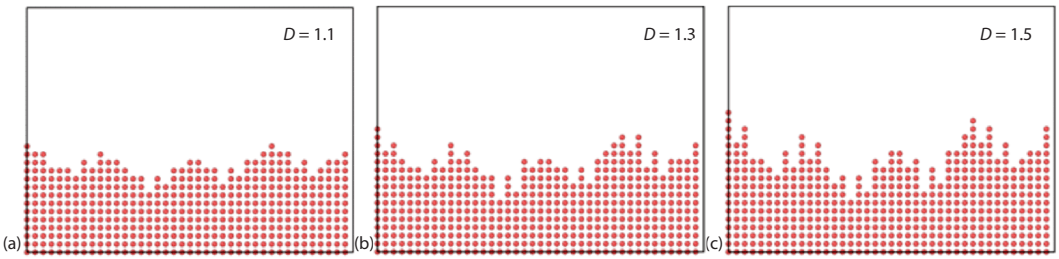

Figure 1. The snapshots of the constructed model for different fractal dimensions (the red particles indicate the isolated carbon atoms); (a) 1.1, (b) 1.3, and (c) 1.5 (*for color image see journal web site*)

Simulation method

The GCMC and MD simulations were performed to use the fast parallel algorithms for the short-range molecular dynamics [11]. The Lennard-Jones potential is used to calculate the van der Waals interactions with a cutoff distance of 13 Å [7, 8] and the cross-interaction

parameters are listed in tab. 1. The simulation temperature, 330 K, was controlled using a Nosé-Hoover thermostat [12]. The pressure was controlled by inserting an appropriate number of CH_4 molecules based on the GCMC simulation. In the GCMC simulation, the equilibrium and production runs are set at the same time, *i. e.* at 1 ns. The fugacity coefficient of CO_2/CH_4 is 0.86/0.48 at 330 K and 20 MPa, calculated using the Soave-Redlich-Kwong state equation [13].

The density of the gases in the box was calculated by dividing the box into small bins in the *x*- and *y*-directions. The average densities $\hat{\rho}_{i,j\in bin}$ and velocities $\hat{v}_{i,j\in bin}$ in the i_{bin} over j_{ps} can be calculated [5]:

Table 1. The force field parameters of the graphite and gases used in the simulation

Atom type	Mass [gmol^{-1}]	ε [kcalmol^{-1}]	σ [Å]
C	12.01	0.056	3.4
CH_4	16.04	0.294	3.751
CO_2	44.01	0.481	3.615

$$\hat{\rho}_{i,j\in bin} = \frac{\sum_{j\in N} m_{ij}}{N\Delta x\Delta y L_z} \tag{2}$$

$$\hat{v}_{i,j\in bin} = \frac{\sum_{j\in N} m_{ij} v_{ij}}{N\sum_{j\in N} m_{ij}} \tag{3}$$

where N is the total number of trajectories collected from the MD production stage, m_{ij} – the mass of the gases, and v_{ij} – velocity of the gases, L_z [nm] – the size of the box in the *z*-direction, and $\Delta x/\Delta y$ [nm] – the widths of the bins in the *x*-, *y*-directions.

Results and discussion

Adsorption ability

The adsorption ability of CO_2/CH_4 is evaluated in the GCMC simulation for slit nanopores with different fractal dimensions, fig. 2. It is reported that the isobaric heat of adsorption of CO_2 is around 26.1-28.7 kJ/mol while it is 18.5-20.7 kJ/mol for CH_4 [14]. As a result, the adsorption capacity of CO_2 is nearly twice that of CH_4, fig. 2(a). For different fractal roughness values, the adsorption capacity is reduced with the increase of fractal dimension (in the order $D = 1.1 > D = 1.3 > D = 1.5$). This is mainly due to the decreasing pore volume along with the increase in the height of the asperities on the nanopore surface.

After the GCMC simulation, the exported model is used to perform the EMD simulation. Figures 2(b)-2(d) show typical examples of the density distribution. Because of the weak interaction with the wall, the density at the center remains constant at 0.0082 mol/cm^3, which is the same as that observed for CH_4 in the bulk phase. Close to the wall, the density of CH_4 rapidly increases, indicating the formation of an adsorption layer both on the smooth and roughed surfaces. The shapes of the adsorption layers on both sides of the nanopores are controlled by the morphology of the wall, figs. 2(b)-2(c). The total thickness of the adsorption layers is approximately 4.2 Å, fig. 2(d).

Generally, the accumulation of the gases is attributed to the attractive potential energy between the gases and pore walls shown in fig. 3. The potential energy in the center is higher than the value of the adsorbed gases. When there is the poor influence of the wall to gases in the bulk phase, the adsorption potential energy of the gases along the surface is much smaller. The adsorbed gases need more kinetic energy to overcome the attraction of the walls.

Thermal diffusion property

The thermal diffusion property, caused by the molecular thermal motion, is calculated from the mean square displacement (MSD) [15]:

$$D_{\text{self}} = \frac{1}{2Bt}\frac{1}{N}\sum_{i=1}^{N}\left[r_i(t) - r_i(0)\right]^2 \tag{4}$$

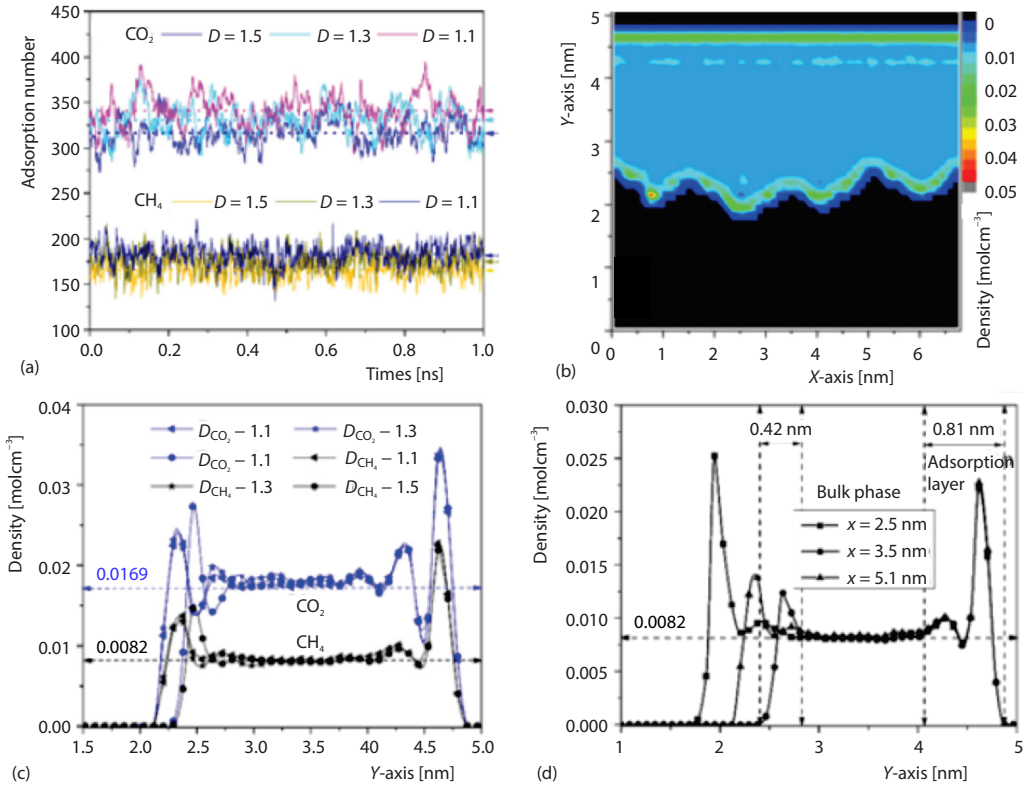

Figure 2. (a) The adsorption capacity of the gases at different fractal dimensions (T = 330 K, P = 20 MPa), (b) a snapshot of density map for CH_4 in nanopores with D = 1.1, (c) density profiles of CH_4/CO_2 in different nanopores, (d) density profiles of CH_4 with x equal to 2.5, 3.5, and 5.1 nm (D = 1.1)

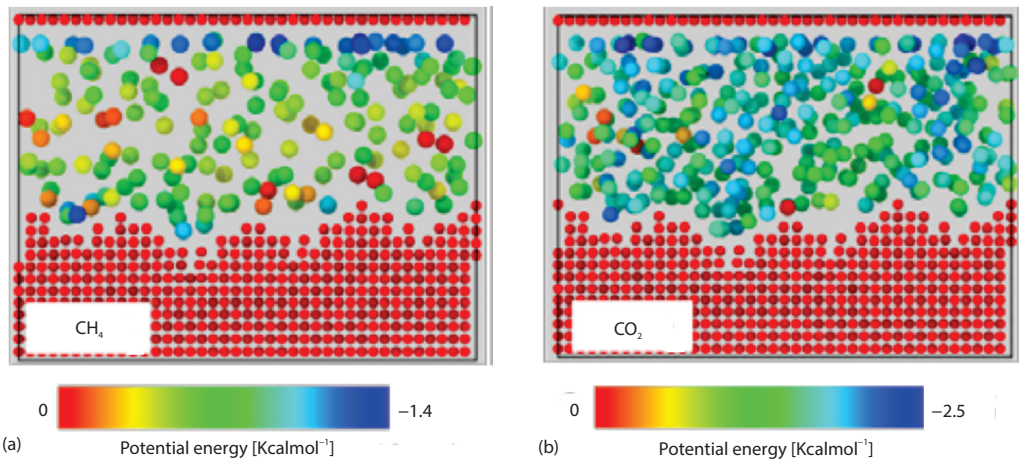

Figure 3. The snapshots of the potential-energy distribution of (a) CH_4, (b) CO_2 in nanopores with D = 1.1

where $B = 1$ is the dimension of the system, $r_i(t)$ – the position at time t, $r_i(t)$ – the initial position, and N – the number of the statistical particles. Because the molecular thermal motion path-

way in the *y*-direction is blocked by the pore wall, the diffusion coefficient in the *y*-direction can be neglected. To study the thermal diffusive ability along the confined nanopores, we plot the MSD of the gases in the *x*-direction in fig. 4.

The diffusion property is consistent with the molecular thermal velocity v [ms^{-1}] [5]. At the same temperature, the thermal speed of CO_2 is only 0.603 times that of CH_4. Moreover, it closes to the molecule-molecule and molecule-wall collision possibilities. Based on the MD simulations, the thermal diffusive coefficient of CH_4 is more than four times that of CO_2, tab. 2. This shows that CO_2 has a higher diffusion speed and can be potentially applied for displacing shale gas based on the molecular dynamic property. For different roughness values, the diffusion coefficient decreases with the increase in the fractal dimension. This is mainly due to the higher collision probability between the gas molecules and the protrusion, which is called the steric hindrance phenomenon [16].

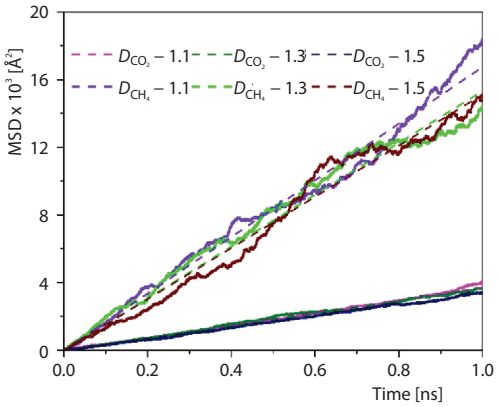

Figure 4. The MSD diagrams of CO_2/CH_4 in the *x*-direction as a function of the simulation time

Table 2. Thermal diffusion property of CO_2/CH_4 in rough nanopores

Gases	CO_2			CH_4		
Fractal dimension, D	1.1	1.3	1.5	1.1	1.3	1.5
Diffusion coefficient $\cdot 10^{-8}$ [m^{2}s^{-1}]	1.85	1.82	1.68	8.38	7.67	7.56
Goodness of fit, R^2	0.998	0.998	0.999	0.995	0.993	0.993

Flow velocity of the fluid

The NEMD simulations are used to evaluate the influence of roughness on the flow of the gases along the pressure gradients in confined nanopores. The pressure gradient is converted to the driving force required to pull gases flow along the nanopores [5]. The relationship between the pressure gradient and driving force can be expressed [5]:

$$nF = \frac{\partial P}{\partial L} = \frac{(P_1 - P_2)}{L} \tag{5}$$

where n is the number of atoms, $F = 0.001$ kcal·mol^{-1}·Å^{-1} is the external force, $\partial P/\partial L$ – the pressure gradient, P_1 and P_2 [MPa] – the pressures at the inlet and outlet of the pore, respectively, and L [m] – the length of the pore. The pressure gradients are same. The velocity is determined by its molecular mass and adsorption ability shown in fig. 5. According to the MD simulation, the velocity of CO_2 is lower than that of CH_4. It is shown that CO_2 can be potentially sequestrated in the organic nanopores.

For the smooth surface, the velocity of the gases is significantly higher than that at other points shown in figs. 5(a)-5(c). The perfectly smooth surface without any intrusion vertical to the flow direction makes the fluid to flow extremely fast. However, the roughness also significantly affects the velocity distribution shown in fig. 5(d). When the value of the fractal dimension change from 1.1-1.5, the velocity of the adsorbed gas decreases to zero due to the

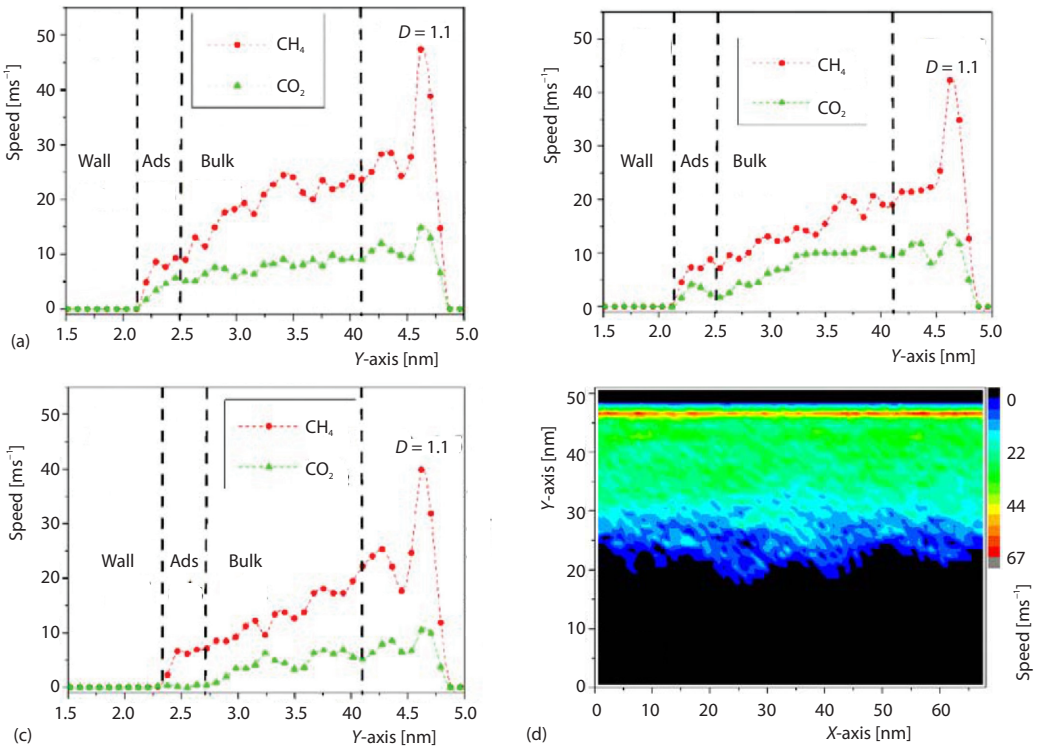

Figure 5. The velocity of CO_2/CH_4 in nanopores with different fractal dimensions: (a) 1.1, (b) 1.3, (c) 1.5, and (d) velocity distribution map of CH_4 in nanopores with $D = 1.1$

longer and the higher collision possibility between the gases and the asperities. In real kerogen pore networks, the surface is usually quit a high roughness values. Thus, CO_2 will be trapped in the shale reservoirs, whereas the fast-moving CH_4 can be recovered.

Conclusion

In our work, the organic-rich nanopores with a fractal surface resembling a real kerogen pore were constructed based on the classic W-M equation by the different values of the fractal dimension. The adsorption ability of CO_2 is nearly twice that of CH_4 due to the different adsorption enthalpy. The thermal diffusion coefficient of CO_2 is only 23.7% that of CH_4 at the same pressure and temperature. The velocity of the adsorbed CO_2 is much smaller than that of CH_4 at the same external pressure gradients due to the higher molecular mass and adsorption ability. The velocity of the adsorbed CO_2 reduced zero when the fractal roughness is increased to 1.5. It is shown that CO_2 has the potential to replace the CH_4 in shale.

Acknowledgment

This work was supported by the Fundamental Research Funds for the Central Universities (2018BSCXB19), the Postgraduate Research Practice Innovation Program of Jiangsu Province (KYCX18_1975).

Nomenclature

D – fractal dimension, [–]
D_{self} – self-diffusion coefficient, [m^2s^{-1}]
F – external force, [N]
G – roughness amplitude, [m]
j – time to collection result, [ns]
m_{ij} – mass of the molecule, [g]
L – length of the pore, [nm]
L_z – size of model in z direction, [nm]
M – molar mass, [$gmol^{-1}$]
N – total number of trajectories
P – pressure, [Pa]
$\partial P/\partial L$ – pressure gradients, [Pam^{-1}]
$r_i(t)$ – molecular position at time t, [m]
$r_i(0)$ – molecular initial position, [m]
t – simulation time, [ns]
v – molecular thermal velocity, [ms^{-1}]
$\hat{v}$ – average velocity, [ms^{-1}]
Δx – size of the bins in x direction, [nm]
Δy – size of the bins in y direction, [nm]

Greek symbols

γ – frequency density, [–]
ρ – average density, [gcm^{-3}]

References

[1] Wu, T., *et al*., Multiscale Pore Structure and Its Effect on Gas Transport in Organic-rich Shale, *Water Resources Research*, *53* (2017), 7, pp. 5438-5450
[2] Patzek, T., *et al*., A Simple Model of Gas Production from Hydrofractured Horizontal Wells in Shales, *Aapg Bulletin*, *98* (2014), 12, pp. 2507-2529
[3] Li, Z., *et al*., Liquid Nitrogen Gasification Fracturing Technology for Shale Gas Development, *Journal of Petroleum Science and Engineering*, *138* (2016), Feb., pp. 253-256
[4] Loucks, R. G., *et al*., Morphology, Genesis, and Distribution of Nanometer-scale Pores in Siliceous Mudstones of the Mississippian Barnett Shale, *Journal of Sedimentary Research*, *79* (2009), 12, pp. 848-861
[5] Wang, S., *et al*., Fast Mass Transport of Oil and Supercritical Carbon Dioxide through Organic Nanopores in Shale, *Fuel*, *181* (2016), Oct., pp. 741-758
[6] Bousige, C., *et al*., Realistic Molecular Model of Kerogen's Nanostructure, Nature Materials, *15* (2016), 5, pp. 576-582
[7] Zhu, X., *et al*., Atomic Mechanisms and Equation of State of Methane Adsorption in Carbon Nanopores, *The Journal of Physical Chemistry C*, *118* (2014), 31, pp. 17737-17744
[8] Castez, M. F., *et al*., Methane Flow Through Organic-rich Nanopores: the Key Role of Atomic-Scale Roughness, *The Journal of Physical Chemistry C*, *121* (2017), 51, pp. 28527-28536
[9] Ju, Y., *et al*., Fractal Model and Lattice Boltzmann Method for Characterization of Non-Darcy Flow in Rough Fractures, *Scientific Reports*, *7* (2017), Mar., pp. 41380
[10] Zeng, Y., *et al*., Gas Transport in Self-affine Rough Micro-Channels of Shale Gas Reservoir, *Journal of Petroleum Science and Engineering*, *167* (2018), Aug., pp. 716-728
[11] Plimpton, S., Fast Parallel Algorithms for Short-Range Molecular Dynamics, *Journal of Computational Physics*, *117* (1993), 1, pp. 1-19
[12] Evans, D. J., *et al*., the Nose-Hoover Thermostat, *Journal of Chemical Physics*, *83* (1985), 8, pp. 4069-4074
[13] Soave, G., Equilibrium Constants from a Modified Redlich-Kwong Equation of State, *Chemical Engineering Science*, *27* (1972), 6, pp 1197-1203
[14] Huang, L., *et al*., Molecular Simulation of Adsorption Behaviors of Methane, Carbon Dioxide and Their Mixtures on Kerogen, Effect of Kerogen Maturity and Moisture Content, *Fuel*, *211* (2018), Jan., pp. 159-172
[15] Kulasinski, K., *et al*., Water Diffusion in Amorphous Hydrophilic Systems: A Stop and Go Process, *Langmuir*, *31* (2015), 39, pp. 10843-10849
[16] Cha, J., *et al*., Molecular Dynamics Simulation of Dispersion Improvement of Graphene Sheets in Nanofluids by Steric Hindrance Resulting from Functional Groups, *Molecular Simulation*, *43* (2016), 3, pp. 228-233

Paper submitted: September 12, 2018
Paper revised: November 20, 2018
Paper accepted: January 25, 2019